Generalizing, optimizing, and inventing numerical algorithms for the fractional Fourier, Fresnel, and linear canonical transforms

Bryan M. Hennelly and John T. Sheridan

Department of Electronic and Electrical Engineering, Faculty of Architecture and Engineering, University College Dublin, Belfield, Dublin 4, Republic of Ireland

Received August 16, 2004; accepted October 11, 2004

By use of matrix-based techniques it is shown how the space–bandwidth product (SBP) of a signal, as indicated by the location of the signal energy in the Wigner distribution function, can be tracked through any quadratic-phase optical system whose operation is described by the linear canonical transform. Then, applying the regular uniform sampling criteria imposed by the SBP and linking the criteria explicitly to a decomposition of the optical matrix of the system, it is shown how numerical algorithms (employing interpolation and decimation), which exhibit both invertibility and additivity, can be implemented. Algorithms appearing in the literature for a variety of transforms (Fresnel, fractional Fourier) are shown to be special cases of our general approach. The method is shown to allow the existing algorithms to be optimized and is also shown to permit the invention of many new algorithms. © 2005 Optical Society of America

OCIS codes: 080.2730, 100.2000, 070.4560, 200.2610, 200.3050, 200.4560, 200.4740.

1. INTRODUCTION

As part of this paper we explicitly discuss more than ten numerical algorithms[1–11] known in the literature that describe different methods of calculating the output of optical systems (including free-space propagation) given some input wave field. We begin our introduction by highlighting this fact because it illustrates (a) the practical importance of these algorithms and (b) what appears to be the complexity of a problem that requires the derivation of so many different numerical techniques. Clearly, the availability of stable fast numerical methods to carry out such calculations are critically important and of general interest.

Here we show that a relatively simple procedure can be used to derive all the previous algorithms. We also show how the existing algorithms can be interpreted and optimized with our approach. Finally, we show that intimate links exist among the following three entities:

1. The optical system, its matrix representation, and the corresponding linear integral transformation.
2. The Wigner distribution function (WDF) of the signal and the signal's space–Bandwidth product (SBP) as it passes through the optical system.
3. The optimum numerical algorithm with which to calculate the effect of such systems.

In overview the paper is organized as follows. In Section 2 we briefly discuss the WDF and its relationship to the SBP and the Nyquist sampling criteria. In Section 3 we discuss the linear canonical transform (LCT) and its integral and matrix definitions. We show how the SBP varies following application of the LCT and how this variation can be determined automatically. In Section 4 we explicitly discuss the matrices and the variations of the SBP for five common optical transforms, the Fourier transform (FT), the fractional Fourier transform (FRT), the Fresnel transform (FST), the chirp modulation transform (CMT), and scaling. In Section 5 we give an overview of the numerical algorithms available, and we represent these as matrices. We then discuss matrix decompositions so that each of the matrices presented in Section 4 can be decomposed into a set of matrices that can be related directly to the numerical algorithms. In Section 6 we show how this methodology can be used to derive some well-known numerical algorithms that have previously appeared in the recent literature. In total ten algorithms are examined, primarily for the calculation of the FRT and FST. We show that all of these algorithms are special cases of our general procedure for deriving LCT algorithms. In Section 7 we invent a number of new algorithms and discuss the possibility of future invention. In Section 8 we offer a conclusion.

2. WIGNER DISTRIBUTION FUNCTIONS AND SPACE–BANDWIDTH PRODUCTS

The WDF of a complex optical amplitude distribution (or Wigner distribution chart) provides a graphical means of simultaneously viewing the signal's spatial and spatial-frequency distributions and is particularly useful for visualizing localized signals.[12–16] $W_u(x,k)$, the WDF of a signal $u(x)$, is defined in terms of this spatial distribution as

$$W_u(x,k) = \psi\{u(x)\}(x,k) = \int_{-\infty}^{\infty} u(x-\xi/2)u^*(x-\xi/2) \times \exp(-j2\pi k\xi)\mathrm{d}\xi, \quad (1)$$

where k represents spatial frequency, * denotes complex conjugation, and $\psi\{u(x)\}(x,k)$ denotes the WDF operator. The real-valued WDF has double the number of dimen-

sions; i.e., a complex one-dimensional signal has a two-dimensional WDF, while two-dimensional signals have four-dimensional WDFs. The WDF is entirely reversible[13,17] with the exception of a constant phase factor as shown in

$$u(x)u^*(0) = \int_{-\infty}^{\infty} W_u(x/2,k)\exp(j2\pi kx)\mathrm{d}k, \tag{2a}$$

$$|u(0)|^2 = \int W_u(0,k)\mathrm{d}k. \tag{2b}$$

An exactly equivalent definition of the WDF can be given by using the FT of $u(x)$, which we denote as $U(k)$, as follows:

$$W_u(x,k) = \int_{-\infty}^{\infty} U\left(k - \frac{\xi}{2}\right)U^*\left(k - \frac{\xi}{2}\right)\exp(j2\pi x\xi)\mathrm{d}\xi. \tag{3}$$

In many practical problems it is assumed that a signal is bounded within some finite region in both the spatial and spatial-frequency domains. The spatial extent W_0 and the frequency extent B_0 are defined[17] such that

$$u(x) \approx 0, \quad |x| > W_0/2, \tag{4a}$$

$$U(k) = \int_{-\infty}^{\infty} u(x)\exp(-j2\pi kx)\mathrm{d}x \approx 0, \quad |k| > B_0/2, \tag{4b}$$

and therefore the signal energy is negligible outside these spatial and spatial-frequency regions. For all signals discussed here W_0 and B_0 may also be defined as follows[17]:

$$\int_{-W_0/2}^{W_0/2} |u(x)|^2\mathrm{d}x = \eta E, \tag{5a}$$

$$\int_{-B_0/2}^{B_0/2} |U(k)|^2\mathrm{d}k = \eta E, \tag{5b}$$

where $\eta \lesssim 1$, and E represents the total signal energy:

$$E = \int_{-\infty}^{\infty} |u(x)|^2\mathrm{d}x = \int_{-\infty}^{\infty} |U(k)|^2\mathrm{d}k. \tag{6}$$

The dual equality in Eqs. (5) follows from Rayleigh's theorem. In Fig. 1(a) we show the WDF of a signal $u(x)$ in which the signal energy lies within a rectangular area. The four corner coordinates that define the shape are shown on the diagram. The signal $u(x)$ is completely determined if it is sampled equidistantly in x with sample space δx such that the Nyquist criterion is satisfied:

$$\delta x \leqslant 1/B_0. \tag{7}$$

Therefore the number of samples N required to describe $u(x)$ completely is

$$N = W_0/\delta x \geqslant W_0B_0. \tag{8}$$

Clearly, for the most efficient uniform sampling $\delta x = 1/B_0$ and $N = W_0B_0$, the SBP of the signal. In general signals may have an irregularly shaped WDF, and one such case is shown in Fig. 1(d). This shape is the result of applying a FST to the signal with regular WDF shown in Fig. 1(a).

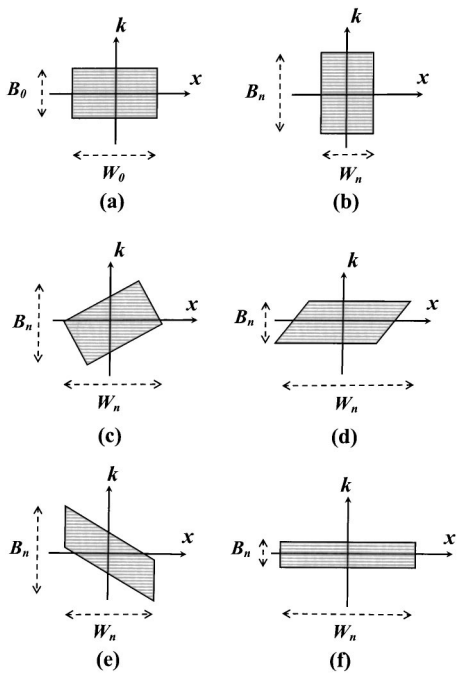

Fig. 1. WDF of a signal before and after different types of LCT are applied to the signal: (a) WDF of the original signal, (b) WDF of the signal after it has been Fourier transformed, (c) WDF of the signal after it has been fractional Fourier transformed, (d) WDF of the Fresnel transformed signal, (e) WDF of the signal after it has been chirp multiplied, (f) WDF of the magnified signal.

Such a signal can be fully described with a number of samples less than the SBP,[17] but this requires nonuniform sampling in the space domain.

3. LINEAR CANONICAL TRANSFORMS, MATRICES, AND SPACE–BANDWIDTH PRODUCT

The LCT[13,16,18] is a three-parameter class of linear integral transform and is defined as follows

$$u_{\alpha,\beta,\gamma}(x') = L_{\alpha,\beta,\gamma}\{u(x)\}(x') = \exp(-j\pi/4)\sqrt{\beta}\int_{-\infty}^{\infty} u(x) \times \exp[j\pi(\alpha x^2 - 2\beta xx' + \gamma x'^2)]\mathrm{d}x, \tag{9}$$

where α, β, and γ are real transform parameters that are independent of the x and x' domain coordinates. This can be further generalized to a five-parameter transform known as the special affine Fourier transform[19,20] (SAFT), in which the additional two parameters are shifts in the spatial and spatial-frequency domain and have no effect on the numerics. The LCT is a unitary transform and includes as special cases the FT, the FST, the FFT, and the operations of scaling (magnification) and chirp multiplication (thin lenses). Optical systems implemented by using an arbitrary number of thin lenses and propagation through free space in the Fresnel approximation, or through sections of graded-index media, belong to the class of systems known as quadratic-phase systems[9] (QPSs). All QPSs can be described mathematically by using the LCT. In our formulation the wavelength factor has been included as a part of α, β, and γ. However, in most

cases in the literature the wavelength is explicitly given as a parameter in the definition of the QPS, since it is common to all three parameters. The effect of the operator $L_{\alpha,\beta,\gamma}$ on the WDF of the signal is

$$W(x,k) \rightarrow W(ax+bk, cx+dk), \tag{10}$$

where $ad-bc=1$, $a=\gamma/\beta$, $b=1/\beta$, $c=-\beta+\alpha\gamma/\beta$, and $d=\alpha/\beta$. This is equivalent to the following matrix transformation acting in phase space:

$$\begin{bmatrix} x' \\ k' \end{bmatrix} = \mathbf{L}\begin{bmatrix} x \\ k \end{bmatrix} = \begin{bmatrix} a & b \\ c & d \end{bmatrix}\begin{bmatrix} x \\ k \end{bmatrix} = \begin{bmatrix} \gamma/\beta & 1/\beta \\ -\beta+\alpha\gamma/\beta & \alpha/\beta \end{bmatrix}\begin{bmatrix} x \\ k \end{bmatrix}. \tag{11}$$

These matrices are unit determinant, implying a conservation of area (energy) on the WDF chart. The matrices are useful because the product of the composition matrices of two or more successive optical systems is the matrix of the overall optical system.

We will show that these matrices can be used to derive efficient algorithms for the numerical calculation of LCTs, but first we develop a formalism to calculate automatically the SBP by using matrix algebra. In Fig. 2 we show the WDFs of a signal and of its LCT. We have assumed that the signal's energy lies within some arbitrary (asymmetrical in $x-k$) four-sided shape that is defined by the corner coordinates (x_1, k_1), (x_2, k_2), (x_3, k_3), and (x_4, k_4). We can, in fact, take any number of such points and sides to define the bounded area in which most of the signal's energy lies. The spatial extent of the signal is W_0, its spatial-frequency bandwidth is B_0, and the number of samples required, with uniform equidistant sampling, to describe the signal fully is $N_0=W_0B_0$. After applying the LCT the shape changes. However, the bounded area, the bounded energy, and the number of sides remains the same as a result of the affine nature of the LCT. The number of samples now required to determine the transformed signal, with uniform equidistant sampling, is given by $N_n=W_nB_n$. With matrix algebra the change in position of each of the four coordinates defining the WDF, and thus W_n and B_n and subsequently N_n, can be found simply as follows. Given

$$\mathbf{S} = \begin{bmatrix} x_1 & x_2 & x_3 & x_4 \\ k_1 & k_2 & k_3 & k_4 \end{bmatrix}, \tag{12a}$$

the new corner coordinates are given by

$$\mathbf{S}' = \mathbf{LS} = \begin{bmatrix} x_1' & x_2' & x_3' & x_4' \\ k_1' & k_2' & k_3' & k_4' \end{bmatrix} = \begin{bmatrix} ax_1+bk_1 & ax_2+bk_2 & ax_3+bk_3 & ax_4+bk_4 \\ cx_1+dk_1 & cx_2+dk_2 & cx_3+dk_3 & cx_4+dk_4 \end{bmatrix}, \tag{12b}$$

where $\mathbf{S}$ and $\mathbf{S}'$ are the corner coordinate matrices (CCM) before and after application of the LCT. The spatial extent is clearly the maximum distance between any two of the x coordinates, while similarly the spatial-frequency bandwidth is the maximum distance between any two of the k coordinates. The spatial extent and the spatial frequency can be automatically obtained from the CCM by using the distances matrix $\mathbf{D}$:

$$\mathbf{D} = \begin{bmatrix} 1 & 1 & 1 & 0 & 0 & 0 \\ -1 & 0 & 0 & 1 & 1 & 0 \\ 0 & -1 & 0 & -1 & 0 & 1 \\ 0 & 0 & -1 & 0 & -1 & -1 \end{bmatrix}. \tag{13}$$

To illustrate this we find W_0 and B_0 of the original signal and define the extent vector $\mathbf{E}$,

$$\mathbf{E} = \begin{bmatrix} W_0 \\ B_0 \end{bmatrix} = \mathrm{Max}|\mathbf{SD}| = \mathrm{Max}\begin{bmatrix} |x_1-x_2| & |x_1-x_3| & |x_1-x_4| & |x_2-x_3| & |x_2-x_4| & |x_3-x_4| \\ |k_1-k_2| & |k_1-k_3| & |k_1-k_4| & |k_2-k_3| & |k_2-k_4| & |k_3-k_4| \end{bmatrix}, \tag{14}$$

where we have introduced the notation Max[–] to denote the maximum element on each row. On the right-hand side of Eq. (14) we find the distance between each possible pair of coordinates in the x (top row) and the k (bottom row). The absolute value of each element is then calculated, giving a 2×6 matrix of positive elements. The maximum value appearing in each of the two rows is determined, giving a 2×1 vector. On the left-hand side of Eq. (14) the element in the top row is W_0 and in the bottom row is B_0. To calculate N_0 we find the product of the transpose and the rotated extent vector as shown in Eq. (14), where $\mathbf{R}$ is the rotation matrix:

$$N_0 = \frac{1}{2}\mathbf{E}^{\mathrm{T}}\mathbf{RE} = \frac{1}{2}[W_0\ B_0]\begin{bmatrix} 0 & 1 \\ 1 & 0 \end{bmatrix}\begin{bmatrix} W_0 \\ B_0 \end{bmatrix} = W_0B_0. \tag{15}$$

After application of the LCT the transformed signal has a new extent vector $\mathbf{E}'$:

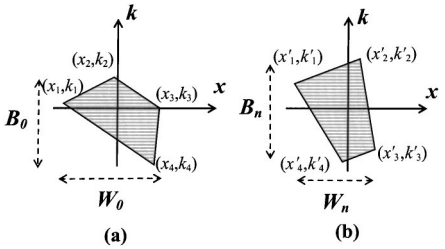

Fig. 2. WDF of a signal with bounded signal energy (a) before and (b) after application of an arbitrary LCT.

$$\mathbf{E}' = \begin{bmatrix} W_n \\ B_n \end{bmatrix} = \mathrm{Max}|\mathbf{S}'\mathbf{D}| = \mathrm{Max}\begin{bmatrix} |a(x_1-x_2)+b(k_1-k_2)| & |a(x_1-x_3)+b(k_1-k_3)| & |a(x_1-x_4)+b(k_1-k_4)| & |a(x_2-x_3)+b(k_2-k_3)| \\ |c(x_1-x_2)+d(k_1-k_2)| & |c(x_1-x_3)+d(k_1-k_3)| & |c(x_1-x_4)+d(k_1-k_4)| & |c(x_2-x_3)+d(k_2-k_3)| \end{bmatrix}$$
$$\begin{bmatrix} |a(x_2-x_4)+b(k_2-k_4)| & |a(x_3-x_4)+b(k_3-k_4)| \\ |c(x_2-x_4)+d(k_2-k_4)| & |c(x_3-x_4)+d(k_3-k_4)| \end{bmatrix}. \quad (16)$$

Earlier we noted that we can take any number of coordinates and sides to define the bounded area in which most of the signal's energy lies. In relation to this, when the WDF is bounded by n sides (with n coordinates) the CCM $\mathbf{S}$ will be of dimension $2\times n$, and the distances matrix $\mathbf{D}$ will be of dimension $n\times(\Sigma_{i=1}^{n-1} i)$. Extension to more than four coordinates is straightforward.

In many cases the original sampled signal (whose LCT we wish to generate numerically) will occupy a regular rectangular shape on the WDF such as that shown in Fig. 1(a). This assumption is used in all of the algorithms[1–11] in the literature. In this case the input CCM is

$$\begin{bmatrix} x_1 & x_2 & x_3 & x_4 \\ k_1 & k_2 & k_3 & k_4 \end{bmatrix} = \begin{bmatrix} -W_0/2 & W_0/2 & W_0/2 & -W_0/2 \\ B_0/2 & B_0/2 & -B_0/2 & -B_0/2 \end{bmatrix}. \quad (17)$$

Clearly, however, this may not always be the case. An example would be if the original signal were a Fresnel-transformed image for which uniform sampling was used in the recording process. Such a signal would have a WDF resembling that shown in Fig. 1(d). In this case we should not automatically assume the CCM given in Eq. (17) and should use whatever *a priori* knowledge is available to define the correct initial elements of the CCM. In Section 5 we will optimize the existing algorithms[11–21] to allow for a nonrectangular initial WDF.

We note that if we do assume an initial rectangle with the CCM defined in Eq. (17) and with the extent vector $\mathbf{E}=\begin{bmatrix} W_0 \\ B_0 \end{bmatrix}$, the extent vector of the signal resulting from the LCT would be

$$\mathbf{E}' = \begin{bmatrix} W_n \\ B_n \end{bmatrix} = \mathrm{Max}\begin{bmatrix} |aW_0| & |bB_0 - aW_0| & |bB_0| & |bB_0 + aW_0| \\ |cW_0| & |dB_0 - cW_0| & |dB_0| & |dB_0 + cW_0| \end{bmatrix}. \quad (18)$$

The largest elements of the two rows in the matrix are clearly dependent on the values of a, b, c, and d (and therefore on the parameters, α, β, and γ of the LCT in question). Once these maximum values are determined it is then possible to calculate the number of equidistant samples required to describe the signals fully.

4. COMMON TRANSFORMS AND CHANGES IN SPACE–BANDWIDTH PRODUCT

In this section we will look at some of the most common forms of LCT and their effect on the shape of the WDF of a signal. This will allow us to determine the change in the number of equidistant samples required to describe the signal after these transforms have been applied. The resulting information will later be applied to derive various numerical algorithms with matrix algebra. We review five transforms, each of which describes an optical system. First, we examine the FT, which can be implemented with a single lens and two sections of free space.[14] Second, we examine the FRT[15,16,19,20], which has numerous applications and optical implementations. Next, we discuss the FST,[14] which corresponds to free-space propagation and is referred to as chirp convolution. Then we review chirp multiplication, which is realized optically by a thin lens. Fifth and finally, we discuss simple scaling or magnification. Many QPSs can be implemented from combinations of these systems (e.g., the first two can be composed from the last three). We will not discuss the applications or optical implementations of these transforms further but proceed to present mathematical definitions and apply the theory outlined in Section 3 to describe the resulting changes in the WDF and SBP.

The optical FT has the integral representation

$$F\{u(x)\}(k) = \int_{-\infty}^{\infty} u(x)\exp\left(-j\frac{2\pi}{\lambda f}xk\right)\mathrm{d}x, \quad (19)$$

where λ is the wavelength of light and f is the focal length of the Fourier transforming lens. Application of the FT causes a rotation of the WDF by $\pi/2$ rad. This is illustrated in Fig. 1(b), where we show the WDF of the Fourier transform of the original signal whose (rectangular symmetric) WDF, with spatial extent W_0 and spatial-frequency bandwidth B_0, is shown in Fig. 1(a). Defining the FT in terms of the LCT parameters gives $\alpha=\gamma=0$, $\beta=1/\lambda f$, and this gives

$$\begin{bmatrix} a & b \\ c & d \end{bmatrix} = \begin{bmatrix} 0 & \lambda f \\ -1/\lambda f & 0 \end{bmatrix}. \quad (20)$$

The normalized FT matrix is given by the same matrix setting $\lambda f=1$. Let us apply the optical FT to a signal with spatial extent W_0, a bandwidth B_0, and $N_0=W_0B_0$. The new extent vector is

$$\mathbf{E}' = \begin{bmatrix} W_n \\ B_n \end{bmatrix} = \begin{bmatrix} \lambda f B_0 \\ W_0/\lambda f \end{bmatrix}, \tag{21}$$

which is true for any input CCM. The new SBP is

$$N_n = W_n B_n = \lambda f B_0 \frac{W_0}{\lambda f} = W_0 B_0 = N_0. \tag{22}$$

Despite the change in the WDF there has been no change in the SBP. The same number of samples can be used to represent the signal before and after application of the optical or normalized FT regardless of the initial CCM.

The optical FRT has the integral representation

$$F_p\{u(x)\}(x_p) = \int_{-\infty}^{\infty} u(x) \exp\left\{ j\frac{\pi}{\lambda q}\left[\frac{x^2}{\tan(p\pi/2)} - \frac{2xx_p}{\sin(p\pi/2)} + \frac{x_p^2}{\tan(p\pi/2)} \right] \right\} \mathrm{d}x, \tag{23}$$

where q is called the standard focal length[15] and is dependent on the physical parameters of the optical FRT system, and p is the order of the FRT and defines the domain x_p into which it transforms. The FRT is defined separately for p equal to integer multiples of 2. When $p=1$ the FRT reduces to the FT, which is simply a special case. Application of the FRT of a given order causes a rotation of the WDF by $p\pi/2$ radians.[15] Such a rotation is illustrated in Fig. 1(c). We define the FRT in terms of the LCT in Eq. (9) with $\alpha=\gamma=1/[\lambda q \tan(p\pi/2)]$ and $\beta=1/[\lambda q \sin(p\pi/2)]$. Thus the matrix for the FRT is

$$\begin{bmatrix} a & b \\ c & d \end{bmatrix} = \begin{bmatrix} \cos(p\pi/2) & \lambda q \sin(p\pi/2) \\ -\sin(p\pi/2)/\lambda q & \cos(p\pi/2) \end{bmatrix}. \tag{24}$$

The extent vector after application of the FRT can now be calculated for any initial CCM [with the most general corner coordinates (x_1, k_1), (x_2, k_2), (x_3, k_3) and (x_4, k_4)] by substituting the known values into Eq. (15). The new SBP can then be calculated with Eq. (14). For the general case E' is algebraically cumbersome, so we do not define it explicitly here. However, in the case of the initial CCM defined by Eq. (16),

$$\mathbf{E}' = \begin{bmatrix} W_n \\ B_n \end{bmatrix} = \begin{bmatrix} B_0 \lambda q |\sin(p\pi/2)| + W_0 |\cos(p\pi/2)| \\ B_0 |\cos(p\pi/2)| + W_0 |\sin(p\pi/2)|/\lambda q \end{bmatrix}, \tag{25}$$

and the new SBP is given by

$$N_n = W_n B_n = N_0 + (1/2)|\sin(p\pi)|(\lambda q B_0^{\,2} + W_0^{\,2}/\lambda q). \tag{26}$$

From Eq. (26) we can deduce that any rotation (when p is not an integer) of the WDF shown in Fig. 1(a) produces an increase in the SBP and therefore an increase in the number of samples needed to represent the signal after application of the FRT. This is caused by changes in the spatial extent and spatial-frequency bandwidth. We note that the values of W_n, B_n, and N_n are periodic in p of period 1. For an initial signal with a general CCM we find the new SBP by using Eqs. (15), (16), and (24), and it is possible that the number of samples we require will decrease.

The third transform we deal with is the FST, which has the integral representation

$$\mathrm{FST}_z\{u(x)\}(x_z) = \int_{-\infty}^{\infty} u(x) \exp\left[j\frac{\pi}{\lambda z}(x^2 - 2xx_z + x_z^{\,2}) \right] \mathrm{d}x, \tag{27}$$

where z is the distance of propagation and x_z is the output Fresnel domain. Application of the FST of a given distance causes a horizontal shearing of the WDF in the space dimension (the amount of shearing dependent on the value of z). This effect is illustrated in Fig. 1(d). Defining the FST in terms of the LCT gives $\alpha=\gamma=\beta=1/\lambda z$ and this gives the (upper triangular) matrix for the FST:

$$\begin{bmatrix} a & b \\ c & d \end{bmatrix} = \begin{bmatrix} 1 & \lambda z \\ 0 & 1 \end{bmatrix}. \tag{28}$$

The extent vector after application of the FST for the most general initial CCM is calculated by substituting the known values into Eq. (16). In the case of the signal shown in Fig. 1(a) the new extent vector is

$$\mathbf{E}' = \begin{bmatrix} W_n \\ B_n \end{bmatrix} = \begin{bmatrix} \lambda z B_0 + W_0 \\ B_0 \end{bmatrix}. \tag{29}$$

The spatial extent increases as z increases, while the bandwidth is unchanged. The new SBP is

$$N_n = N_0 + \lambda z B_0^{\,2}. \tag{30}$$

The horizontal shearing of the WDF has increased the SBP and therefore increased the number of samples needed to represent the signal after application of the FST. For the most general CCM the bandwidth will always remain constant at B_0 but the spatial extent can increase or decrease depending on the elements of the CCM.

The fourth transform is the chirp modulation transform (CMT), which describes the physical process of passing through a thin lens in the paraxial approximation. It has the integral form

$$CM\{u(x)\}(x) = \int_{-\infty}^{\infty} u(x') \exp\left(-j\frac{\pi}{\lambda f} x'^2 \right) \delta(x - x') \mathrm{d}x' = u(x) \exp\left(-j\frac{\pi}{\lambda f} x^2 \right), \tag{31}$$

where f is the focal length of the lens and δ denotes the Dirac delta function. Positive and negative values of f correspond to positive and negative lenses, respectively. Application of the CMT causes a vertical shearing of the WDF along the frequency axis. This effect is illustrated in Fig. 1(e). The effect of the CMT on the WDF is a direct result of the following property of the WDF[13,16]:

$$\psi\{u(x)g(x)\}(x,k) = \int W_u(x, k-k') W_g(x,k') \mathrm{d}k'. \tag{32}$$

From this we can derive a lower triangular matrix for the CMT on the WDF (for a positive lens) as

$$\begin{bmatrix} a & b \\ c & d \end{bmatrix} = \begin{bmatrix} 1 & 0 \\ -1/\lambda f & 1 \end{bmatrix}. \tag{33}$$

The extent vector after application of the CMT for the most general initial CCM is calculated by substituting the known values into Eq. (15). This is given explicitly in Eq. (34a) below since it is used often in deriving the later algorithms. In the case of the signal shown in Fig. 1(a) the new extent vector is presented in Eq. (34b).

$$\mathbf{E}' = \mathrm{Max}\begin{bmatrix} |(x_1 - x_2)| & |(x_1 - x_3)| & |(x_1 - x_4)| & |(x_2 - x_3)| \\ |(x_2 - x_1)/\lambda f + (k_1 - k_2)| & |(x_3 - x_1)/\lambda f + (k_1 - k_3)| & |(x_4 - x_1)/\lambda f + (k_1 - k_4)| & |(x_3 - x_2)/\lambda f + (k_2 - k_3)| \end{bmatrix}$$

$$\begin{bmatrix} |(x_2 - x_4)| & |(x_3 - x_4)| \\ |(x_4 - x_2)/\lambda f + (k_2 - k_4)| & |(x_4 - x_3)/\lambda f + (k_3 - k_4)| \end{bmatrix}, \tag{34a}$$

$$\mathbf{E}' = \begin{bmatrix} W_n \\ B_n \end{bmatrix} = \begin{bmatrix} W_0 \\ B_0 + W_0/\lambda f \end{bmatrix}. \tag{34b}$$

In the general case of Eq. (34a) the spatial extent remains constant while the bandwidth changes. In the case of Eq. (34b) the bandwidth increases and the shorter the focal length, the greater the increase in bandwidth. The new SBP will therefore increase and is given by

$$N_n = N_0 + W_0{}^2/\lambda f \tag{35}$$

The vertical shearing of the WDF has brought about an increase in the SBP. This is entirely caused by a change in the bandwidth and not in the spatial extent. As we decrease f, we increase the number of samples required to describe the CMT signal. For the most general CCM and the extent vector of Eq. (34a), the spatial width will always remain the same. However, the bandwidth can increase–decrease depending on the elements of the CCM, and there will be a corresponding increase–decrease in the number of samples required for the signal.

The final transform we consider in overview is scaling, which is also called magnification (demagnification) or squeezing and is typically realized in imaging systems.[13,14,16] The scaling operation has the integral representation

$$M_M\{u(x)\}(x) = \sqrt{1/M}\int_{-\infty}^{\infty} u(x')\,\delta(x - x'/M)dx' = \sqrt{1/M}\,u(x/M), \tag{36}$$

where M is the magnifying factor of the imaging system in question. $M>1$ corresponds to magnification and $M<1$ to demagnification. Scaling causes an elongation of the WDF. The effect of demagnification is illustrated in Fig. 1(f). The matrix is derived by use of the following definition of the Dirac delta function[13,16]:

$$\delta(x) = \lim_{y\to\infty}\left\{ y^{-1/2}\exp\left[j\pi\left(\frac{x^2}{y} - \frac{1}{4}\right)\right]\right\}, \tag{37}$$

and is given by

$$\begin{bmatrix} a & b \\ c & d \end{bmatrix} = \begin{bmatrix} M & 0 \\ 0 & 1/M \end{bmatrix}. \tag{38}$$

The extent vector (regardless of the initial CCM) after scaling is

$$\mathbf{E}' = \begin{bmatrix} W_n \\ B_n \end{bmatrix} = \begin{bmatrix} MW_0 \\ B_0/M \end{bmatrix}. \tag{39}$$

The spatial extent scales by a factor of M as does the bandwidth. The new SBP therefore does not change, and the same number of samples is needed to describe the signal.

$$N_n = (MW_0)(B_0/M) = N_0. \tag{40}$$

In this section we have examined the effect of the FT, FRT, FST, CMT and scaling on the WDF. The resulting changes in the WDF change the SBP and therefore the number of uniform samples necessary to represent the signal satisfactorily. Applying this technique, we can now systematically sample in the input and output domains in a way that is intimately linked to the optical system. For the FT and scaling we have deduced that there will be no change in the number of samples required in the input and output domains. This result is true for any initial shape (CCM) of the WDF. However, for the FRT, FST, and CMT the initial CCM shape determines whether we need to increase or decrease the number of samples required to describe the output signal.

5. NUMERICAL PROCESSES AND THEIR ASSOCIATED MATRICES

In this section we discuss the numerical processes available in the literature. In particular we discuss the FFT, scaling, and numerical chirp multiplication. We assign a matrix representation to each of these three numerical processes. These three tools are the only tools to simulate the LCT. In Section 6 we will proceed to examine the subject of matrix decompositions, which will allow us to de-

compose the LCT matrices discussed in previous sections into products of these three matrices, each of which corresponds to the numerical processes that we can use.

The most widely used computational algorithm in optical transform simulation is the FFT.[21] The FFT has been used to calculate the FT,[14] FRT,[1–4] and FST.[5–11] The FFT is an efficient means of determining the discrete Fourier transform with $N \log N$ calculations instead of the N^2 calculations that would otherwise be required. The savings in the number of calculations is large if N is large. The FFT takes N input samples and outputs N samples that are approximations to the sample values of the continuous FT of the original function. The matrix for the normalized FT, $\begin{bmatrix} 0 & 1 \\ -1 & 0 \end{bmatrix}$, can be numerically implemented with the FFT. Since the continuous FT has no effect on the SBP, Eq. (22)—the FFT algorithm—efficiently maps N input samples (with sampling interval δx) to N output samples (with sampling interval $\delta k = 1/N\delta x$). In each instance in this paper where the FFT is used, we assume that a discrete function in the range $-N/2 \leqslant n \leqslant N/2-1$ is mapped to a discrete function in the range $-N/2 \leqslant m \leqslant N/2-1$. In general, for ease of computation the FFT maps from the range $0 \leqslant n \leqslant N-1$ to $0 \leqslant m \leqslant N-1$. If such an FFT algorithm is used, then we must wrap the output function around such that the last $N/2$ samples become the first $N/2$ and vice versa, and we must also multiply every odd sample by -1.

The scaling operation also has no effect on the SBP and involves no additional computational cost. Therefore, it affects only the sampling intervals δx and δk in the x and k domains, i.e.,

$$\delta x \rightarrow M\delta x, \tag{41}$$

$$\delta k \rightarrow \delta k/M. \tag{42}$$

These changes in sampling intervals correspond to the changes in spatial extent and bandwidth shown in Eq. (38).

Numerical implementation of chirp multiplication is somewhat more difficult. The matrix shown in Eq. (33) is numerically implemented by multiplying each sample of the discrete function by complex values as shown in relation (43), where $-N/2 \leqslant n \leqslant N/2-1$:

$$f(n\delta x) \rightarrow f(n\delta x)\exp\left[-\frac{j2\pi}{\lambda f}(n\delta x)^2\right], \tag{43}$$

where $\delta x = W_0/N$. The CMT brings about a change in the bandwidth of the signal it operates on while it leaves the spatial extent unchanged. This results in a corresponding change in the number of samples required to describe the signals, which in turn depends on the elements of the CCM of the discrete function being operated on. In the case where CMT causes an increase in bandwidth (and therefore a subsequent increase in the SBP and the number of samples required to represent the signal), we accommodate by interpolating the input samples. If the CMT gives $B_n = kB_0$ (and $N_n = kN_0$), where $k > 1$, we must interpolate or upsample by a factor of k. Interpolation can be carried out with numerous methods,[22] e.g., by using two FFT algorithms of size N_n. In the case where the CMT causes a decrease in bandwidth (and therefore a decrease in the number of samples required to represent the signal), we accommodate by decimating the input samples. If the CMT gives $B_n = kB_0$ (and $N_n = kN_0$), where $k < 1$, we must decimate or downsample by a factor of k.[22] In the case where the new SBP is not an integer value we should round to the nearest integer so that interpolation–decimation may be applied.

In Section 6 we will show that algorithms to generate LCTs can be derived by using matrix decomposition in which we decompose the LCT matrix into a product of scaling, FT, and CMT matrices, each of which has numerical implementations. To account for the changes in SBP we must track the changes in the CCM, finding the new extent vector at each stage. This means that we must track the CCM as it passes through each component matrix in the algorithm so that we know exactly what happens as it passes through the CMT matrix of interest. We note that in some cases it is possible that the CMT may actually reduce the SBP, for example when the CMT reverses the effect of an earlier CMT operation.

Thus far we have examined the numerical implementation of three types of matrices, corresponding to the FT, scaling, and chirp multiplication. We now apply the theory of matrix decomposition to other types of matrices that match other types of LCT, such as the FRT and FST and finally the most general form of the LCT with arbitrary parameters. The goal is to decompose these more complicated matrices into products of the matrices examined in this section and then use their numerical implementations.

6. SYSTEMATIC GENERALIZATIONS AND OPTIMIZATIONS OF EXISTING ALGORITHMS

In this section we show that the existing algorithms used for simulation of the FST, FRT, and LCT[1–11] can be derived efficiently by using our technique of matrix decomposition and tracking of the CCM and the extent vector (and therefore the SBP) as the signal passes through the decomposed matrices.

In the literature, there are restrictive conditions placed on the accurate use of each of these algorithms. For example, the direct method[5,8] for implementing the FST is accurate for large distances z, and conversely the spectral method[5,8] for implementing the FST is accurate for small distances. These conditions will not be listed here since, in all cases, we show these conditions can be removed by employing interpolation and extrapolation. We show that the various algorithms for implementation of the FST all give identical outputs if they are used correctly. The difference between them is the number of calculations used and the degree of interpolation and extrapolation required to obtain these results. The same conclusions apply to the various algorithms for calculation of the FRT.[1–4] We also show that all the FRT algorithms can be made index additive.

The subject of matrix decomposition has been investigated extensively in the literature.[23–25] In the case of the optical FT the following decomposition is well known:

$$\begin{bmatrix} 0 & \lambda f \\ -1/\lambda f & 0 \end{bmatrix} = \begin{bmatrix} \lambda f & 0 \\ 0 & 1/\lambda f \end{bmatrix} \begin{bmatrix} 0 & 1 \\ -1 & 0 \end{bmatrix}. \tag{44}$$

Therefore the optical FT can be numerically implemented with a single FFT algorithm followed by a scaling of the output-sampling interval; the number of calculations for a discrete input function of N samples is $N \log N$.

The FST has a number of different numerical implementations. The direct method[5,8] can be derived by use of the following matrix decomposition for the FST:

$$\begin{bmatrix} 1 & \lambda z \\ 0 & 1 \end{bmatrix} = \begin{bmatrix} 1 & 0 \\ 1/\lambda z & 1 \end{bmatrix} \begin{bmatrix} \lambda z & 0 \\ 0 & 1/\lambda z \end{bmatrix} \begin{bmatrix} 0 & 1 \\ -1 & 0 \end{bmatrix} \begin{bmatrix} 1 & 0 \\ 1/\lambda z & 1 \end{bmatrix} = \mathbf{M}_4\mathbf{M}_3\mathbf{M}_2\mathbf{M}_1. \tag{45}$$

$\mathbf{M}_1$ corresponds to a CMT and will induce a change in the number of samples required to describe the input function $u_0(n\delta x)$ with N_0 samples and a CCM $\mathbf{S}_0$, where $\delta x = W_0/N_0$. The new number of samples N_1 is found by using the new extent vector $\mathbf{E}_1 = \mathrm{Max}|\mathbf{M}_1\mathbf{S}_0\mathbf{D}|$ [see Eqs. (12a) and (13)] and multiplying the elements of $\mathbf{E}_1$, (W_1 and B_1) together. We interpolate or decimate u_0 depending on the value of N_1. Next we multiply by the quadratic chirp factor as shown in relation (43), where $\delta x = W_0/N_1$, $N_1/2 \leqslant n \leqslant N_1/2-1$, and $f=-z$. Next appears the matrix product $\mathbf{M}_3\mathbf{M}_2$, which corresponds to an optical FT whose implementation has previously been discussed; the required number of samples remains N_1. $\mathbf{M}_4$ is a second CMT, and the number of samples changes to N_4, which is calculated from the last extent vector $\mathbf{E}_4 = \mathrm{Max}|\mathbf{M}_4\mathbf{M}_3\mathbf{M}_2\mathbf{M}_1\mathbf{S}_0\mathbf{D}|$, and we apply interpolation or decimation as required [$\mathbf{E}_4$ is equivalent to that given in Eqs. (34)]. We multiply by the quadratic chirp factor as shown in relation (43), where $\delta x = W_3/N_4$, $N_4/2 \leqslant n \leqslant N_4/2-1$, $f=-z$, and W_3 is the first element of $\mathbf{E}_3 = \mathrm{Max}|\mathbf{M}_3\mathbf{M}_2\mathbf{M}_1\mathbf{S}_0\mathbf{D}|$, the extent vector after application of the third matrix. We note that if only the amplitude of the FST is required, we can neglect $\mathbf{M}_4$ since it affects only the phase.

The next algorithm we deal with is the spectral method for the calculation of the FST.[5,8] The matrix decomposition is as follows:

$$\begin{bmatrix} 1 & \lambda z \\ 0 & 1 \end{bmatrix} = \begin{bmatrix} 0 & -1 \\ 1 & 0 \end{bmatrix} \begin{bmatrix} 1 & 0 \\ -\lambda z & 1 \end{bmatrix} \begin{bmatrix} 0 & 1 \\ -1 & 0 \end{bmatrix} = \mathbf{M}_3\mathbf{M}_2\mathbf{M}_1. \tag{46}$$

$\mathbf{M}_1$ is calculated with a single FFT algorithm, and the number of samples remains the same. $\mathbf{M}_2$ is a CMT, and the number of samples changes to N_2, which is calculated from the $\mathbf{E}_2 = \mathrm{Max}|\mathbf{M}_2\mathbf{M}_1\mathbf{S}_0\mathbf{D}|$; we apply interpolation or decimation as required. We multiply by the quadratic chirp factor as shown in relation (43), where $\delta x = W_1/N_2$, $N_2/2 \leqslant n \leqslant N_2/2-1$, $\lambda f = 1/\lambda z$, and W_1 is the first element of $\mathbf{E}_1 = \mathrm{Max}|\mathbf{M}_1\mathbf{S}_0\mathbf{D}|$, the extent vector after application of the second matrix. Finally we apply a second FFT algorithm to implement $\mathbf{M}_3$. If correct interpolation and decimation are applied when implementing the direct and spectral methods, both methods give identical results, outputting the same number of samples with the same values. For small values of z, the direct method is numerically intensive because of the rapid oscillation of the chirp factor and the subsequent need for large interpolation, which can be seen on the WDF as a large vertical shearing. In this case the last chirp factor causes decimation and reduces the number of samples. The spectral method does not undergo such dramatic interpolation–decimation stages and is preferable for small z. For large z the reverse is true and the direct method becomes the preferred method particularly in the case where we require only the amplitude of the FST.

The Rhodes light tube method[9,10] requires only a single algorithm for all z when implementing the FST. The matrix decomposition is

$$\begin{bmatrix} 1 & \lambda z \\ 0 & 1 \end{bmatrix} = \begin{bmatrix} M & 0 \\ 0 & 1/M \end{bmatrix} \begin{bmatrix} 1 & 0 \\ 1/\lambda f_2 & 1 \end{bmatrix} \begin{bmatrix} 1 & \lambda z_T \\ 0 & 1 \end{bmatrix} \begin{bmatrix} 1 & 0 \\ 1/\lambda f_1 & 1 \end{bmatrix} = \mathbf{M}_4\mathbf{M}_3\mathbf{M}_2\mathbf{M}_1, \tag{47}$$

where we have the conditions $z_T = f_1 + f_2$, $M = 1 - z_T/f_2$, $z = Mz_T$, with f_1 and f_2 chosen arbitrarily. $\mathbf{M}_1$ is a CMT, which changes the number of samples. Taking $\mathbf{S}_0$ to be the input CCM, the new number of samples N_1 is found by using the new extent vector $\mathbf{E}_1 = \mathrm{Max}|\mathbf{M}_1\mathbf{S}_0\mathbf{D}|$. We interpolate or decimate depending on the value of N_1. Next we multiply by the quadratic chirp factor as shown in relation (43), where $\delta x = W_0/N_1$, $N_1/2 \leqslant n \leqslant N_1/2-1$, and $f = f_1$. Then we implement $\mathbf{M}_2$ using the spectral method algorithm, Eq. (46). $\mathbf{M}_3$ is a second CMT and the number of samples changes to N_3, which is calculated from $\mathbf{E}_3 = \mathrm{Max}|\mathbf{M}_3\mathbf{M}_2\mathbf{M}_1\mathbf{S}_0\mathbf{D}|$, and we apply interpolation or decimation as required. We multiply by the quadratic chirp factor as shown in relation (43), where $\delta x = W_3/N_3$, $N_3/2 \leqslant n \leqslant N_3/2-1$, $f = f_2$, and W_3 is the first element of $\mathbf{E}_3 = \mathrm{Max}|\mathbf{M}_3\mathbf{M}_2\mathbf{M}_1\mathbf{S}_0\mathbf{D}|$, the extent vector after application of the third matrix. The fourth matrix $\mathbf{M}_4$ simply scales the sampling interval. In Refs. 18 and 20 the initial CCM is taken to be the rectangular one defined by Eq. (17) and f_1 is taken to be $W_0/\lambda B_0$. The result is that the spatial width of the signal does not change through $\mathbf{M}_2$, i.e., $W_2 = W_0$, and thus the wave field remains inside the spatial "light tube." This method can be viewed as a numerical extension of the idea of superresolution.[26–28] Once again, if correct interpolation and decimation are applied when implementing the FST by the direct, spectral, or light tube method, all methods give identical results, outputting the same number of samples with the same values.

We have examined three algorithms for implementing the FST. Now we deal with the FRT. A method for fast implementation of the optical FRT was presented in Ref. 4. The corresponding matrix decomposition is

$$\begin{bmatrix} \cos\phi & \lambda q \sin\phi \\ -\sin\phi/\lambda q & \cos\phi \end{bmatrix} = \begin{bmatrix} 1 & 0 \\ \dfrac{1}{\lambda q \tan\phi} & 1 \end{bmatrix} \times \begin{bmatrix} \lambda q \sin\phi & 0 \\ 0 & 1/\lambda q \sin\phi \end{bmatrix} \times \begin{bmatrix} 0 & 1 \\ -1 & 0 \end{bmatrix} \begin{bmatrix} 1 & 0 \\ \dfrac{1}{\lambda q \tan\phi} & 1 \end{bmatrix} = \mathbf{M}_4\mathbf{M}_3\mathbf{M}_2\mathbf{M}_1, \tag{48}$$

where $\phi=p\pi/2$ and p is the fractional order. We note the similarity between this and the decomposition for the direct method for the FST in Eq. (45). The discussion regarding the numerical implementation is identical in both cases and will not be repeated. However, we note that for small orders, even though the FRT matrix will bring about only a small change in space bandwidth product, $\mathbf{M}_1$ will require a large interpolation, which is later offset by $\mathbf{M}_4$, which in turn gives rise to a closely equivalent amount of decimation. We note that if only the amplitude of the FRT is required we can ignore the presence of $\mathbf{M}_4$ since it affects only the phase.

A similar algorithm is derived in Ref. 1 for implementation of the normalized FRT. The matrix decomposition is the same as Eq. (48), setting $\lambda q=1$. To derive this algorithm we apply the same argument as in the previous case.

In Ref. 2 an FRT algorithm is derived by substituting Shannon's interpolation formula into the integral definition for the FRT, thus obtaining a convolution summation that can be calculated by the FFT. The matrix decomposition for this algorithm is

$$\begin{bmatrix} \cos\phi & \sin\phi \\ -\sin\phi & \cos\phi \end{bmatrix} = \begin{bmatrix} 1 & 0 \\ T-S & 1 \end{bmatrix}\begin{bmatrix} 0 & -1 \\ 1 & 0 \end{bmatrix}\begin{bmatrix} 1 & 0 \\ -1/S & 1 \end{bmatrix} \times \begin{bmatrix} 0 & 1 \\ -1 & 0 \end{bmatrix}\begin{bmatrix} 1 & 0 \\ T-S & 1 \end{bmatrix} = \mathbf{M}_5\mathbf{M}_4\mathbf{M}_3\mathbf{M}_2\mathbf{M}_1, \tag{49}$$

where $S=1/\sin(p\pi/2)$ and $T=1/\tan(p\pi/2)$. The algorithm derived in Ref. 2 is limited to the case where the input function is scaled such that the function occupies a circle on the WDF. However, the matrix decomposition above offers a novel interpretation of this algorithm and allows us to extend its use to the more general case. $\mathbf{M}_1$ is a CMT that changes the number of samples. Once again we take $\mathbf{S}_0$ to be the input CCM, and we find the new number of samples N_1 by finding the new extent vector $\mathbf{E}_1=\mathrm{Max}|\mathbf{M}_1\mathbf{S}_0\mathbf{D}|$. We interpolate or decimate u_0 depending on the value of N_1 compared with N_0. Then we multiply by the quadratic chirp factor as shown in relation (43), with $\delta x=W_0/N_1$, $N_1/2\leqslant n\leqslant N_1/2-1$, and $f=1/\lambda(S-T)$. Next we implement $\mathbf{M}_2$ with an FFT algorithm. $\mathbf{M}_3$ is a second CMT, and the number of samples changes to N_3, which is calculated from $\mathbf{E}_3=\mathrm{Max}|\mathbf{M}_3\mathbf{M}_2\mathbf{M}_1\mathbf{S}_0\mathbf{D}|$, where we apply interpolation or decimation as required. We multiply by the quadratic chirp factor as shown in relation (43), where $\delta x=W_3/N_3$, $N_3/2\leqslant n\leqslant N_3/2-1$, $f=-S/\lambda$, and W_3 is the first element of $\mathbf{E}_3=\mathrm{Max}|\mathbf{M}_3\mathbf{M}_2\mathbf{M}_1\mathbf{S}_0\mathbf{D}|$, the extent vector after application of the third matrix. The fourth matrix $\mathbf{M}_2$ is implemented with an FFT algorithm. $\mathbf{M}_5$ is a third CMT identical to the first. The number of samples becomes N_5, which is calculated from the last extent vector $\mathbf{E}_5=\mathrm{Max}|\mathbf{M}_5\mathbf{M}_4\mathbf{M}_3\mathbf{M}_2\mathbf{M}_1\mathbf{S}_0\mathbf{D}|$, and we apply interpolation or decimation as required. We multiply by the quadratic chirp factor as shown in relation (43), where $\delta x=W_4/N_5$, $N_5/2\leqslant n\leqslant N_5/2-1$, $f=1/\lambda(S-T)$, and W_4 is the first element of $\mathbf{E}_4=\mathrm{Max}|\mathbf{M}_4\mathbf{M}_3\mathbf{M}_2\mathbf{M}_1\mathbf{S}_0\mathbf{D}|$. For small orders $\mathbf{M}_1$ will require a large interpolation, which is later offset by $\mathbf{M}_5$. If only the amplitude of the FRT is required we can $\mathbf{M}_5$. Although it is not explicitly stated in Ref. 2, this algorithm can also be used to implement the optical FRT in an identical manner with the same matrix decomposition setting $S=1/\lambda q\sin(p\pi/2)$ and $T=1/\lambda q\tan(p\pi/2)$.

In Ref. 3 an algorithm is derived based on the Lohmann Type II optical implementation of the FRT,[15] which consists of a lens of focal length f followed by free-space propagation of a distance z followed by a second lens of focal length f. For fractional order p, standard focal length q, and wavelength λ we set $f=q/\tan(p\pi/4)$ and $z=q\sin(p\pi/2)$. The matrix decomposition is

$$\begin{bmatrix} \cos\phi & \lambda q\sin\phi \\ -\sin\phi/\lambda q & \cos\phi \end{bmatrix} = \begin{bmatrix} 1 & 0 \\ -1/\lambda f & 1 \end{bmatrix}\begin{bmatrix} 0 & -1 \\ 1 & 0 \end{bmatrix}\begin{bmatrix} 1 & 0 \\ -\lambda z & 1 \end{bmatrix} \times \begin{bmatrix} 0 & 1 \\ -1 & 0 \end{bmatrix}\begin{bmatrix} 1 & 0 \\ -1/\lambda f & 1 \end{bmatrix} = \mathbf{M}_5\mathbf{M}_4\mathbf{M}_3\mathbf{M}_2\mathbf{M}_1 \tag{50}$$

It can be shown that Eqs. (49) and (50) are identical. This leads us to an interesting conclusion: The algorithms presented in Refs. 2 and 3 are essentially the same even though they are derived in very different ways, and the numerical implementation of Eq. (50) is the same as that for Eq. (49).

We conclude our discussion of FRT algorithms by making three important points that concern all FRT algorithms:

1. As stated in Refs. 2–4 FRTs of small order p will lead to large amounts of interpolation and decimation in each of the algorithms, which can be avoided by carrying out the FRT algorithm for an order $(p+1)$ and then applying an inverse FFT algorithm. The matrix decomposition is

$$\begin{bmatrix} \cos(p\pi/2) & \lambda q\sin(p\pi/2) \\ -\sin(p\pi/2)/\lambda q & \cos(p\pi/2) \end{bmatrix} = \begin{bmatrix} 0 & -\lambda q \\ 1/\lambda q & 0 \end{bmatrix} \times \begin{bmatrix} \cos[(p+1)\pi/2] & \lambda q\sin[(p+1)\pi/2] \\ -\sin[(p+1)\pi/2]/\lambda q & \cos[(p+1)\pi/2] \end{bmatrix}. \tag{51}$$

Eq. (51) applies to the normalized (setting $\lambda q=1$) and the optical FRT.

2. A desirable property of any FRT algorithm is that it be invertible, i.e., applying the algorithm for order p and then applying it for order-p should recover the original discrete function. If the CCM is tracked through the matrix decomposition such that we apply sufficient interpolation and decimation, then the original discrete function can always be completely recovered by carrying out the inverse algorithm. However, it is important to retain the CCM at the end of the forward transform and use it as the input CCM for the second algorithm.

3. Another desirable property of any FRT algorithm is that it be index additive, i.e., applying the algorithm of order p_1 and then applying a second of order p_2 should give the same output as if we had applied a single algorithm of order (p_1+p_2). If the CCM is tracked through the matrix decomposition of the first algorithm for order p_1 and used as the input CCM for the second algorithm of order p_2,

and—what is important—if appropriate interpolation and decimation are applied, then this property will exist.

Before proceeding we return briefly to our discussion of FST algorithms. In Ref. 5 an algorithm for implementing the FST for all distances z is derived that uses the FRT algorithm presented in Ref. 3. The matrix decomposition is

$$\begin{bmatrix} 1 & \lambda z \\ 0 & 1 \end{bmatrix} = \begin{bmatrix} 1/\cos\phi & 0 \\ 0 & \cos\phi \end{bmatrix} \begin{bmatrix} 1 & 0 \\ \tan\phi/\lambda q & 1 \end{bmatrix} \times \begin{bmatrix} \cos\phi & \lambda q \sin\phi \\ -\sin\phi/\lambda q & \cos\phi \end{bmatrix} = \mathbf{M}_3\mathbf{M}_2\mathbf{M}_1, \quad (52)$$

where $q \tan\phi = z$. $\mathbf{M}_1$ is calculated with the algorithm defined by Eq. (50). We note that if we were to calculate $\mathbf{M}_1$ with the algorithm defined by Eq. (48), then Eq. (52) would be reduced to the direct method defined by Eq. (45). After implementing $\mathbf{M}_1$ the number of samples is N_1. $\mathbf{M}_2$ is a CMT that again changes the number of samples. The new number of samples N_2 is found by use of the extent vector $\mathbf{E}_2 = \mathrm{Max}|\mathbf{M}_2\mathbf{M}_1\mathbf{S}_0\mathbf{D}|$. We interpolate or decimate depending on the values of N_1 and N_2. Next we multiply by the quadratic chirp factor as shown in relation (43), where $\delta x = W_1/N_2$, $N_2/2 \leq n \leq N_2/2 - 1$, and $f = -q/\tan\phi$. The presence of $\mathbf{M}_3$ means that we change the sampling interval. If only the amplitude of the FST is required we can ignore the presence of $\mathbf{M}_2$, since it affects only the phase.

In Ref. 7 three algorithms are discussed for the numerical calculation of FST when convergent illumination is used. The algorithm is represented by the decomposition

$$\begin{bmatrix} 1 & \lambda z \\ 0 & 1 \end{bmatrix} \begin{bmatrix} 1 & 0 \\ -1/\lambda z_c & 1 \end{bmatrix} = \mathbf{M}_2\mathbf{M}_1. \quad (53)$$

$\mathbf{M}_1$ is a CMT and we find the new number of samples N_1 using the extent vector $\mathbf{E}_1 = \mathrm{Max}|\mathbf{M}_1\mathbf{S}_0\mathbf{D}|$. We interpolate or decimate appropriately. Next we multiply by the quadratic chirp factor as shown in relation (43), where $\delta x = W_0/N_1$, $N_1/2 \leq n \leq N_1/2 - 1$, and $f = z_c$. $\mathbf{M}_2$ is implemented with $\mathbf{M}_1\mathbf{S}_0$ as the input CCM for one of the three FST algorithms already defined in Eqs. (45), (46), and (52). Depending on the initial CCM the presence of the convergent illumination (i.e., $\mathbf{M}_1$) will lead to additional interpolation or decimation than when the FST algorithms are used on their own.

We note that initially we may oversample the input data so that interpolation steps may be avoided at stages throughout the algorithm. This procedure has been used in many of the existing algorithms. If this is used we should use two input CCMs—the CCM of the original function and the CCM of the oversampled function. The two CCMs may be compared at the different stages of the algorithm to see if further interpolation is required or if decimation may be applied at later stages in the algorithm to reduce the number of calculations required.

7. INVENTING NUMERICAL ALGORITHMS FOR THE LINEAR CANONICAL TRANSFORM

In this section we list two matrix decompositions for the general LCT that lead to numerous algorithms based on the methods discussed in Section 6. The first LCT decomposition is

$$\begin{bmatrix} a & b \\ c & d \end{bmatrix} = \begin{bmatrix} 1 & 0 \\ c/a & 1 \end{bmatrix} \begin{bmatrix} a & 0 \\ 0 & 1/a \end{bmatrix} \begin{bmatrix} 1 & b/a \\ 0 & 1 \end{bmatrix} = \mathbf{M}_3\mathbf{M}_2\mathbf{M}_1. \quad (54)$$

$\mathbf{M}_1$ represents a FST that can be implemented with any of the FST algorithms previously discussed, and we note that it produces a change in the number of samples. We note that in general b will be modulated by λ, and the FST matrix will have the same form as those encountered earlier. The presence of $\mathbf{M}_2$ means that we scale the sampling interval. $\mathbf{M}_3$ is a CMT that again changes the number of samples. The new number of samples N_3 is found with the extent vector $\mathbf{E}_3 = \mathrm{Max}|\mathbf{M}_3\mathbf{M}_2\mathbf{M}_1\mathbf{S}_0\mathbf{D}|$. We interpolate or decimate depending on the values of N_2 and N_3. Next we multiply by the quadratic chirp factor as shown in relation (43), where $\delta x = W_2/N_3$, $N_3/2 \leq n \leq N_3/2 - 1$, and $f = -a/\lambda c$. $\mathbf{M}_3$ can be ignored if we require only the amplitude of the output.

The second LCT decomposition is

$$\begin{bmatrix} a & b \\ c & d \end{bmatrix} = \begin{bmatrix} 1 & 0 \\ 1/\lambda f & 1 \end{bmatrix} \begin{bmatrix} m & 0 \\ 0 & 1/m \end{bmatrix} \begin{bmatrix} \cos\phi & \lambda q \sin\phi \\ -\sin\phi/\lambda q & \cos\phi \end{bmatrix} = \mathbf{M}_3\mathbf{M}_2\mathbf{M}_1, \quad (55)$$

where we set $m \cos\phi = a$, $mq\lambda \sin\phi = b$, and we choose f such that $a/\lambda f - \sin\phi/mq\lambda = c$. $\mathbf{M}_1$ represents an optical FRT and can be implemented with any of the FRT algorithms previously discussed; again, there will be a change in the number of samples. The presence of $\mathbf{M}_2$ means that we scale the sampling interval. $\mathbf{M}_3$ is a CMT that changes the number of samples. The new number of samples N_3 is found with the extent vector $\mathbf{E}_3 = \mathrm{Max}|\mathbf{M}_3\mathbf{M}_2\mathbf{M}_1\mathbf{S}_0\mathbf{D}|$. We interpolate or decimate depending on the values of N_2 and N_3. Next, we multiply by the quadratic chirp factor of relation (43), where $\delta x = W_2/N_3$, $N_3/2 \leq n \leq N_3/2 - 1$, and $f = -a/\lambda c$. $\mathbf{M}_3$ can be ignored if we require only the amplitude of the output. Many other possible matrix decompositions exist, and all can be applied in a similar way.

8. CONCLUSIONS

A relatively simple and easily automated method is introduced to track the space–bandwidth product (SPB) of a signal as it passes through an arbitrary quadratic-phase system (QPS) and undergoes deformations of its Wigner distribution function (WDF). Once the SBP can be automatically tracked, the optimum uniform sampling necessary to simulate the signal numerically at every stage in the system can be found. Detailed knowledge of the SBP evolution allows the appropriate up (interpolation) or down (decimation) sampling necessary to be easily identified.

We apply this method to examine and organize numerical implementations of linear canonical transforms (LCT) in the literature, in particular those for the Fresnel (FST), Fourier (FT) and fractional Fourier transforms (FRTs). We clarify the relationships between the numerical algorithms based on the decomposition of the total system matrix in terms of the product of three types of matrices.

Each of the three matrices represents a particular optical process and each appearance of a matrix results in a specific numerical operation in the resulting numerical algorithms. The matrices correspond to Fourier transformation, magnification and chirp multiplication. In the resulting numerical implementations they correspond to the use of the fast Fourier transform (FFT), a change in sampling spacing, and decimation–interpolation operations, respectively.

By applying this technique, we have shown how numerical algorithms to simulate optical systems can be used most efficiently for any given input function, i.e., WDF shape. We have demonstrated the ability to generate numerical algorithms exhibiting additive and unitary properties. Finally, having clarified the link between the matrix decompositions and numerical algorithms for LCTs, we provide a framework for the derivation of new numerical algorithms.

We believe the results presented here provide a complete description of numerical algorithms for QPSs. Furthermore, the presented synthesis of optical system, signal processing, and numerical algorithm concepts provides many potential benefits and insights.

Note added in proof: Recently an N log N algorithm based purely on the shifting properties of the LCT has been proposed.[29] This algorithm is independent of the FFT algorithm, and the matrix that represents it numerically is simply the *ABCD* matrix for the continuous LCT. We are currently comparing this algorithm with those listed in this paper.

ACKNOWLEDGMENTS

We acknowledge the support of Enterprise Ireland and Science Foundation Ireland through the Research Innovation Fund and the Basic Research Programme and of the Irish Research Council for Science, Engineering and Technology.

Corresponding author J. Sheridan may be reached by telephone at +353-(0)1-716-1927, by fax at +353-(0)1-283-0921, by e-mail at John.Sheridan@ucd.ie, and at http://www.ucd.ie/eleceng.

REFERENCES

1. T. Erseghe, P. Kraniauskas, and G. Cariolaro, "Unified fractional Fourier transform and sampling theorem," IEEE Trans. Signal Process. **47**, 3419–3423 (1999).
2. H. M. Ozaktas, O. Arikan, M. A. Kutay, and G. Bozdagi, "Digital computation of the fractional Fourier transform," IEEE Trans. Signal Process. **44**, 2141–2150 (1996).
3. J. Garcia, D. Mas, and R. G. Dorsch, "Fractional Fourier transform calculation through the fast Fourier transform algorithm," Appl. Opt. **35**, 7013–7018 (1996).
4. F. J. Marinho and L. M. Bernardo, "Numerical calculation of fractional Fourier transforms with a single fast Fourier transform algorithm," J. Opt. Soc. Am. A **15**, 2111–2116 (1998).
5. D. Mas, J. Garcia, C. Ferreira, L. M. Bernardo, and F. Marinho, "Fast algorithms for free-space diffraction patterns calculation," Opt. Commun. **164**, 233–245 (1999).
6. M. Sypek, "Light propagation in the Fresnel region. New numerical approach," Opt. Commun. **116**, 43–48 (1995).
7. D. Mas, J. Perez, C. Hernandez, C. Vazquez, J. J. Miret, and C. Illueca, "Fast numerical calculation of Fresnel patterns in convergent systems," Opt. Commun. **227**, 245–258 (2003).
8. D. Mendlovic, Z. Zalevsky, and N. Konforti, "Computation considerations and fast algorithms for calculating the diffraction integral," J. Mod. Opt. **44**, 407–414 (1997).
9. W. T. Rhodes, "Light tubes, Wigner diagrams and optical signal propagation simulation," in *Optical Information Processing: A Tribute to Adolf Lohmann*, H. J. Caulfield, ed. (SPIE Press, Bellingham, Wash., 2002), pp. 343–356.
10. W. T. Rhodes, "Numerical simulation of Fresnel-regime wave propagation: the light tube model," in *Wave-Optical Systems Engineering*, F. Wyrowski, ed., Proc. SPIE **4436**, 21–26 (2001).
11. X. Deng, B. Bihari, J. Gang, F. Zhao, and R. T. Chen, "Fast algorithm for chirp transforms with zooming-in ability and its applications," J. Opt. Soc. Am. A **17**, 762–771 (2000).
12. E. Wigner, "On the quantum correction for thermodynamic equilibrium," Phys. Rev. **40**, 749–759 (1932).
13. M. J. Bastiaans, "Application of the Wigner distribution function in optics," in *The Wigner Distribution—Theory and Applications in Signal Processing*, W. Mecklenbrauker and F. Hlawatsch, eds. (Elsevier Science, Amsterdam, 1997).
14. J. Goodman, *Introduction to Fourier Optics*, 2nd ed. (McGraw-Hill, New York, 1996).
15. A. W. Lohmann, "Image rotation, Wigner rotation and the fractional Fourier transform," J. Opt. Soc. Am. A **10**, 2181–2186 (1993).
16. H. M. Ozaktas, Z. Zalevsky, and M. A. Kutay, *The Fractional Fourier Transform with Applications in Optics and Signal Processing* (Wiley, Hoboken, N.J., 2001).
17. A. W. Lohmann, R. G. Dorsch, D. Mendlovic, Z. Zalevsky, and C. Ferreira, "Space–bandwidth product of optical signals and systems," J. Opt. Soc. Am. A **13**, 470–473 (1996).
18. M. J. Bastiaans, "Wigner distribution function and its application to first-order optics," J. Opt. Soc. Am. **69**, 1710–1716 (1979).
19. S. Abe and J. T. Sheridan, "Generalization of the fractional Fourier transformation to an arbitrary linear lossless transformation: an operator approach," J. Phys. A **27**, 4179–4187 (1994); Corrigenda, 7937–7938 (1994).
20. S. Abe and J. T. Sheridan, "Optical operations on wave functions as the Abelian subgroups of the special affine Fourier transformation," Opt. Lett. **19**, 1801–1803 (1994).
21. J. W. Cooley and J. W. Tukey, "An algorithm for the machine calculation of complex Fourier series," Math. Comput. **19**, 297–301 (1965).
22. R. E. Crochiere and L. R. Rabiner, "Interpolation and decimation of digital signals—A tutorial review," Proc. IEEE **69**, 300–331 (1981).
23. M. Nazarathy and J. Shamir, "First-order optics—a canonical operator representation: lossless systems," J. Opt. Soc. Am. **72**, 356–364 (1982).
24. A. Papoulis, "Ambiguity function in Fourier optics," J. Opt. Soc. Am. **64**, 779–788 (1974).
25. A. Papoulis, *Signal Analysis* (McGraw-Hill, New York, 1977).
26. Z. Zalevsky, D. Mendlovic, and A. W. Lohmann, "Understanding superresolution in Wigner space," J. Opt. Soc. Am. A **17**, 2422–2429 (2000).
27. D. Mendlovic and A. W. Lohmann, "Space–bandwidth product adaptation and its application to superresolution: fundamentals," J. Opt. Soc. Am. A **14**, 558–562 (1997).
28. D. Mendlovic, A. W. Lohmann, and Z. Zalevsky, "Space–bandwidth product adaptation and its application to superresolution: examples," J. Opt. Soc. Am. A **14**, 563–567 (1997).
29. B. M. Hennelly and J. T. Sheridan, "Fast numerical algorithm for the linear canonical transform," J. Opt. Soc. Am. A **22**, 928–937 (2005).